SUPPLEMENTARY METHODS

CT-scanning

The material used in this section comes from the Zooparc de Beauval in France and the Oceanogràfic of Valencia. All the animals were anaesthetized and underwent a computerized tomography for routine matters of each center. The material used is: *Procyon lotor* ZPB_PL_003, and *Zalopus californianus* ZPB_ZC_004 *and Phoca vitulina* OV_PV_001.

The computed tomography at the Oceanographic institution of Valencia (Spain) were performed with Soamatom Volume Access (Siemens). At the French institution of Zooparc de Beauval, the specimens were scanned using a Philips Brillance 64 machine. Supplementary Data 19 shows the acquisition parameters of the tomographic process. The parameters used in each CT-scan for collecting the data are shown in Supplementary Data 19.

Virtual dissection of the specimens

To obtain the surface area of the epaxial and hypaxial muscles at each slice we used the following protocol: (i) we applied enhancement filters to the stack of 16-bit TIFF images using ImageJ v.1.53t, (http://rsbweb.nih.gov/ij/)[1-3]. The resulting images are prepared for enhanced visualization of muscle components. In this case, the images are not converted to 8 bits as in previous works[3], and we used the 16 bits images for the correct visualization of muscles and other tissue components. The segmentation process was performed using the 3D slicer software v. 5.2.2 (www.slicer-org)[4]. In medial position within each vertebra, one slice per vertebra was segmented to collect the distribution of the epaxial and hypaxial muscles along the spine from C1 to the last lumbar, 27 slices in total. The segmentation data for the epaxial and hypaxial muscles were saved in DICOM format. These data were imported into ImageJ. In both cases, all images were normalized at 0.5% and the histogram was adjusted to the range of interest (ROI) using the semiautomatic brightness/contrast tool of ImageJ[1,2]. Applying the *thresholding tool* to select the areas of interest and the binary tool, we convert the stack of images into binary images. The last step is to calculate the areas of each slice automatically with the *Analyze particles tool* from the Analyze menu in ImageJ[1,2]. The results obtained for the areas in mm2 of the epaxial and hypaxial muscles are shown in Supplementary Data 20-22.

Supplementary figures

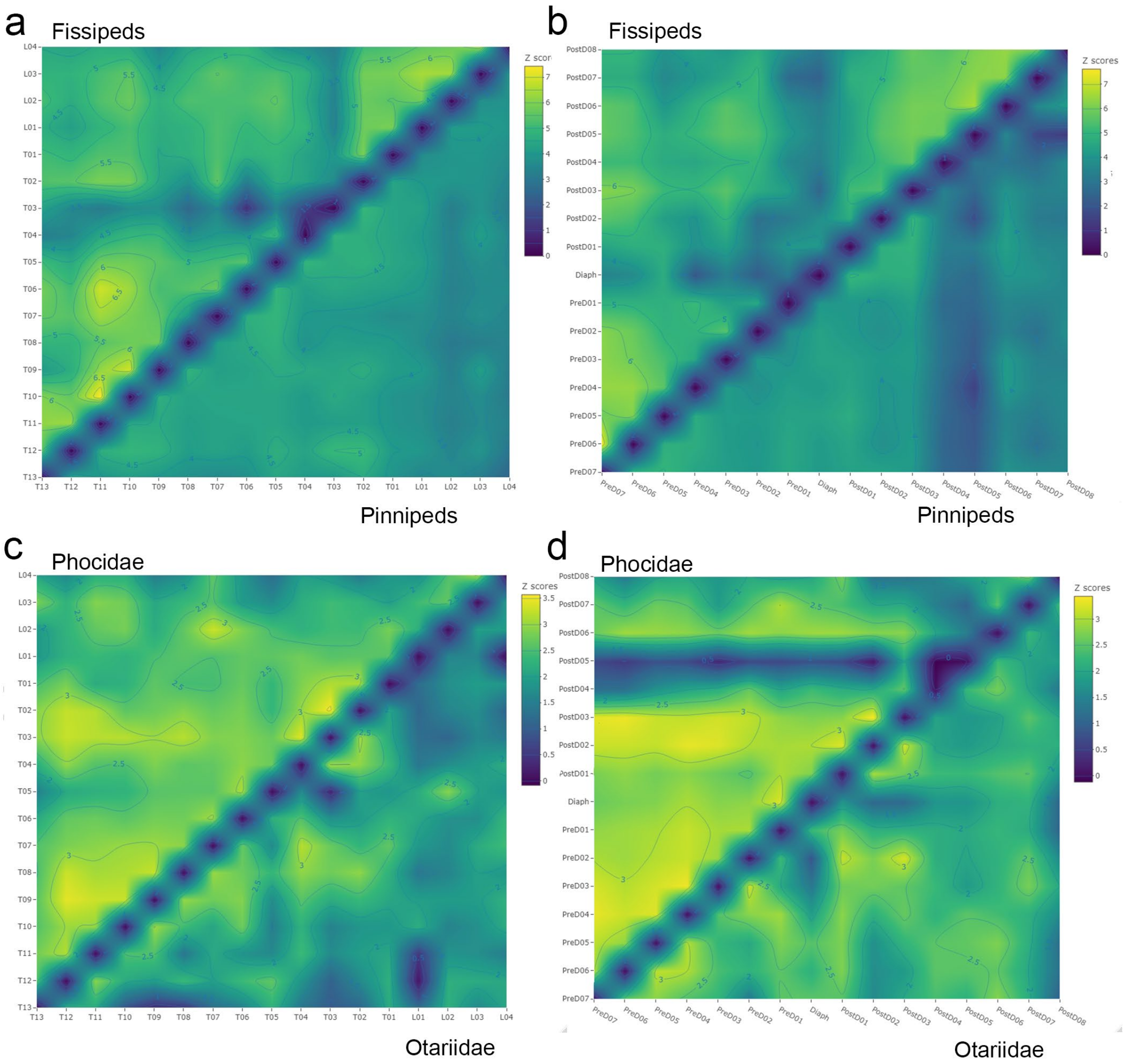

Figure S1. Heatmaps showing the strength of integration between each pair of presacral vertebrae. (A) strength of integration of fissipeds and crown pinnipeds using the "thoracolumbar boundary count" count procedure. The upper semimatrix corresponds to the Z-scores of fissipeds, all taken from ref.16 and the lower semimatrix to the Z-scores of pinnipeds obtained in this study. (B) strength of integration of fissipeds and pinnipeds using the "Diaphragmatic start" count procedure. The upper semimatrix corresponds to the Z-scores of fissipeds taken from Martín-Serra et al.[16], and the lower semimatrix to the Z-scores of pinnipeds obtained in this study. (C) strength of integration of phocids and otariids using the "thoracolumbar boundary count r" count procedure. Upper and lower semi-matrixes correspond to Z-values of phocids and otariids, respectively. (D) strength of integration of phocids and otariids using the "Diaphragmatic start" count procedure. Upper and lower semi-matrixes correspond to Z-values of phocids and otariids, respectively.

Supplementary tables and references

Table S1. Specimens included in the study. Museum abbreviation: LACM, Natural History Museum of Los Angeles County (LA, USA); MNHN, Muséum National d'Histoire Naturelle (Paris, France); NHMB, Natural History Museum of Basel (Basel, Switzerland); ZMUC, Zoological Museum of the University of Copenhagen (Copenhagen, Denmark); AMNH, American Museum of Natural history; NMS, National Museum of Scotland.

Species	**Specimen ID**	**Family**	**Museum**
Odobenus rosmarus ♀	150	Odobenidae	ZMUC
Odobenus rosmarus ♂	n/a	Odobenidae	NHMB
Arctocephalus australis	100341	Otariidae	AMNH
Arctocephalus galapagoensis	100319	Otariidae	AMNH
Arctocephalus gazella ♀	ZMUC 944	Otariidae	ZMUC
Arctocephalus gazella	ZMUC 1081	Otariidae	ZMUC
Arctocephalus pusilus	NA	Otariidae	AMNH
Arctocephalus townsendi	76844	Otariidae	AMNH
Callorhinus ursinus	AMNH 1878-198	Otariidae	AMNH
Eumatopias jubatus	NA	Otariidae	MNHN
Neophoca cinerea ♂	ZMUC 838	Otariidae	ZMUC
Otaria flavescens	ZMUC 148	Otariidae	ZMUC
Otaria flavescens ♂	ZMUC 854	Otariidae	ZMUC
Zalophus californianus	ZMUC 263	Otariidae	ZMUC
Zalophus californianus	ZMUC 384	Otariidae	ZMUC
Zalophus wollebaeki	63957	Otariidae	AMNH
Cystophora cristata ♂	ZMUC 1134	Phocidae	ZMUC

Erignathus barbatus	ZMUC 958	Phocidae	ZMUC
Erignathus barbatus	ZMUC 809	Phocidae	ZMUC
Erignathus barbatus	ZMUC 974	Phocidae	ZMUC
Halichoerus grypus	ZMUC 416	Phocidae	ZMUC
Halichoerus grypus	ZMUC 455	Phocidae	ZMUC
Halichoerus grypus	ZMUC 975	Phocidae	ZMUC
Halichoerus grypus ♂	ZMUC 976	Phocidae	ZMUC
Histriophoca fasciata	NA	Phocidae	AMNH
Leptonychotes weddellii	34250	Phocidae	AMNH
Mirounga angustirostris	ZMUC 839	Phocidae	ZMUC
Mirounga leonina	ZMUC 957	Phocidae	ZMUC
Monachus monachus	73607	Phocidae	AMNH
Monachus schauinslandi ♀	NA	Phocidae	AMNH
Monachus tropicalis	10431	Phocidae	LACM
Phoca groendlandica ♂	ZMUC 780	Phocidae	ZMUC
Phoca groendlandica ♂	ZMUC 782	Phocidae	ZMUC
Phoca groendlandica ♂	ZMUC 961	Phocidae	ZMUC
Phoca largha	15817	Phocidae	AMNH
Phoca vitulina	M180/02	Phocidae	NMS
Phoca vitulina	ZMUC 160	Phocidae	ZMUC
Phoca vitulina	ZMUC 1077	Phocidae	ZMUC
Pusa hispida	ZMUC 157	Phocidae	ZMUC
Pusa hispida	ZMUC 783	Phocidae	ZMUC
Pusa hispida	ZMUC 803	Phocidae	ZMUC
Pusa hispida	ZMUC 950	Phocidae	ZMUC
Pusa sibirica	185595	Phocidae	AMNH

Table S2. Landmark descriptions.

Landmark	Definition
1	Most dorsal point of the spinous process in the cranial side
2	Base of the spinous process in the cranial side
3	Mid-point of the neural arch in the cranial side
4	Right pre-zygapophysis most caudal point
5	Right pre-zygapophysis, most cranial point
6	Right pre-zygapophysis, most lateral-mid point,
7	Right pre-zygapophysis, most medial-mid point
8	Left pre-zygapophysis, most caudal point
9	Left pre-zygapophysis, most cranial point
10	Left pre-zygapophysis, most lateral-mid point
11	Left pre-zygapophysis, most medial-mid point
12	Dorsal point of the cranial facet of the vertebra body
13	Ventral point of the cranial facet of the vertebra body
14	Right-middle point of the cranial facet of the vertebra body
15	Left-middle point of the cranial facet of the vertebra body
16	Cranial point, right transverse process
17	Cranial point, left transverse process
18	Most dorsal point of the spinous process in the caudal side
19	Base of the spinous process in the caudal side
20	Mid-point of the neural arch in the caudal side
21	Left post-zygapophysis, most cranial point
22	Left post-zygapophysis, most caudal point
23	Left post-zygapophysis, most lateral-mid point
24	Left post-zygapophysis, most medial-mid point
25	Right post-zygapophysis, most cranial point
26	Right post-zygapophysis, most caudal point
27	Right post-zygapophysis, most lateral-mid point

28	Right post-zygapophysis, most medial-mid point
29	Dorsal point of the caudal facet of the vertebra body
30	Ventral point of the caudal facet of the vertebra body
31	Left-middle point of the caudal facet of the vertebra body
32	Right-middle point of the caudal facet of the vertebra body
33	Caudal point on the left transverse process
34	Caudal point on the right transverse process
35	Cranial right point on the ventral crest
36	Cranial left point on the ventral crest
37	Cranial middle point on the ventral crest
38	Caudal right point on the ventral crest
39	Caudal left point on the ventral crest
40	Caudal middle point on the ventral crest

Supplementary references

1. Schneider, C.A., Rasband, W.S. & Eliceiri, K.W. NIH Image to ImageJ: 25 325 years of image analysis. Nat. methods. **9**, 671-675 (2012).

2. Pérez-Ramos, A. & Figueirido, B. Toward an “Ancient” virtual World: improvement methods on X-ray CT data processing and virtual reconstruction of fossil skulls. *Front. Earth. Sci.* **8**, 345 (2020).

3. Figueirido, B., Lautenschlager, S., Pérez-Ramos, A. & Van Valkenburgh, B. Distinct predatory behaviors in scimitar-and dirk-toothed sabertooth cats. *Curr. Biol*. **28**, 3260-3266 (2018).

4. Kikinis, R., Pieper, S.D. & Vosburgh, K.G. 3D Slicer: a platform for subject327 specific image analysis, visualization, and clinical support. Intraoperative imaging and 328 image-guided therapy (ed, Jolesz FA) 277-289 (Springer New York, 2014).